ISSN 1990-7931, Russian Journal of Physical Chemistry B, 2024, Vol. 18, No. 4, pp. 1199–1216. © Pleiades Publishing, Ltd., 2024.

CHEMICAL PHYSICS OF NANOMATERIALS

Effect of Implanted Titanium, Vanadium or Chromium on Boron Nitride Surface for Increasing Carbon Monoxide Adsorption: Designing Gas Sensor for Green Chemistry Future

F. Mollaamin[a], *, ** and M. Monajjemi[b]

[a] *Department of Biomedical Engineering, Faculty of Engineering and Architecture, Kastamonu University, Kastamonu, Turkey*

[b] *Department of Chemical Engineering, Central Tehran Branch, Islamic Azad University, Tehran, Iran*

**e-mail: fmollaamin@kastamonu.edu.tr*

***e-mail: smollaamin@gmail.com*

Received January 27, 2024; revised March 27, 2024; accepted May 20, 2024

Abstract—Adsorption of toxic gas of carbon monoxide (CO) molecules by using transition metals (TM) of titanium (Ti), vanadium (V) or chromium (Cr)-doped boron nitride (B_5N_{10}) nanocage have been investigated using density functional theory. The partial density of states can evaluate a determined charge assembly between gas molecules and TM–B_4N_{10} which indicates the competition among dominant complexes of Ti, V, Cr. Based on nuclear quadrupole resonance analysis, TM-doped on B_5N_{10} has shown the lowest fluctuation in electric potential and the highest negative atomic charge including 0.5883 (chromium), 0.6893 (vanadium) and 0.7499 coulomb (titanium), respectively, have presented the most tendency for being the electron acceptors. Furthermore, the reported results of nuclear magnetic resonance spectroscopy have exhibited that the yield of electron accepting for doping atoms on the TM–B_4N_{10} through gas molecules adsorption can be ordered as: Cr > V > Ti that exhibits the strength of covalent bond between titanium, vanadium, chromium, and CO towards toxic gas removal from air. In fact, the adsorption of CO gas molecules can introduce spin polarization on the TM–B_4N_{10} which specifies that these surfaces may be employed as magnetic scavenging surface as a gas detector. Regarding IR spectroscopy, doped nanocages of Ti–B_4N_{10}, V–B_4N_{10}, and Cr–B_4N_{10}, respectively, have the most fluctuations and the highest adsorption tendency for gas molecules which can address specific questions on the individual effect of charge carriers (gas molecule-nanocage), as well as doping atoms on the overall structure. Based on the results of ΔG^{o}_{ads} amounts in this research, the maximum efficiency of Ti, V, Cr atoms doping of B_5N_{10} for gas molecules adsorption depends on the covalent bond between CO molecules and TM–B_4N_{10} as a potent sensor for air pollution removal. Therefore, for a given number of carbon donor sites in CO, the stabilities of complexes owing to doping atoms of Ti, V, Cr can be considered as: CO@Cr–B_4N_{10} > CO@V–B_4N_{10}> CO@Ti–B_4N_{10}.

Keywords: gas detection, nanomaterials, transition metals, density functional theory

DOI: 10.1134/S1990793124700519

INTRODUCTION

The privileged attributes of boron nitrides especially structural and electronic have been made them proper for pollutant adsorption and semiconducting property [1–6]. Boron nitride nanomaterials usually exhibits semi-leading behavior, which is considered a proper alternative to carbon nanotubes. The properties of boron and nitrogen atoms which are the first neighbors of carbon in the periodic table, make boron nitride an interesting subject of numerous studies [7–9]. In recent years, different investigations on the adsorption of chemical contaminants and applying various boron nitride nanostructures as adsorbents for water purification have been studied [10–12]. Various physical shapes of boron nitride (BN)-based nano adsorbents such as nanoparticles, fullerenes, nanotubes, nanofibers, nanoribbons, nanosheets, nanomeshes, nanoflowers, and hollow spheres have been broadly considered possible adsorbents owing to their exceptional characteristics such as large surface area, structural variability, great chemical/mechanical strength, abundant structural defects, high reactive sites, and functional groups [13, 14].

The interactions between carbon monoxide and boron nitride nanocage were investigated using two density functional theory (DFT) functionals (B3LYP and B97D), and 6-31G(*d*) basis set. The computational results indicated the capability of $B_{12}N_{12}$ as a

sensor for potential applications in the detection of CO under an external electric field [15–17]. Ammar H.Y. et al. have studied the effect of transition metals of magnesium and iron doping the boron nitride nanocage ($B_{12}N_{12}$) for adsorption of CO, NO, and NH_3 gases through the electrical and optical properties using by DFT-D3 and TD-DFT calculations at B3lyp/6-311+g(*d*) level of the theory. They found binding energy, ionization potential, electron affinity, chemical hardness, and softness are estimated to emphasize the stability of the doped $MnB_{11}N_{12}$ and $FeB_{11}N_{12}$ [18].

Adsorption involving charged adsorbates causes a change in the double layer and the potential at the outer Helmholtz plane, influencing the adsorption rates of both anodic and cathodic reactions [19–23]. The first three modes are intimately with adsorption and the double layer involves interaction of the adsorbates and the intermediate products [24–27]. These compounds have been formed during the partial electrochemical reactions and interaction of the adsorbed intermediates with organic molecules which can either inhibit or enhance electrode reaction rate. Particularly, this research work aims to assess the influences of doping atoms of Ti, V, Cr on the B_5N_{10} for increasing gas detection through measurement of some parameters containing charge transfer, electric potential, electromagnetic and thermodynamic properties, surface area, functional group and examine the removal of selected toxic gas molecules of carbon monoxide during adsorption process. These discoveries are supposed to open up new nanosensors [28–36] in applications for selective sensing of carbon monoxide in future detecting implementation.

MATERIALS AND METHODS

Carbon Monoxide Molecules Adsorption on TM–B_4N_{10}

Boron nitride nanocage was modeled in the presence of doping atoms of Ti, V, or Cr which can increase the gas sensing potential of BN-nanocage. Therefor, (Ti, V, Cr)-doped B_5N_{10} might be suggested as CO removal from air through an eco-friendly approach (Fig. 1). In our research, sample characterization was performed by CAM–B3LYP–D3/EPR-3, LANL2DZ level.

Figure 1 has shown the process of CO adsorption on the TM–B_4N_{10} surface which towards formation of complexes containing CO@B_5N_{10}, CO@Ti–B_4N_{10}, CO@V–B_4N_{10}, CO@Cr–B_4N_{10} by molecular modeling computations with mutiplicity of 2, 1, 2, 1, respectively. The charge distribution of mentioned complexes is calculated due to the Bader charge analysis [37]. The trapping of CO molecules by TM–B_4N_{10} were successfully incorporated due to binding formation consisting of C → Ti, C → V, C → Cr (Fig. 1).

Application of Density Functional Theory Approach

Hohenberg–Kohn (HK) functions have rigidly made the electronic density permissible as fundamental variable to electronic and structure computations. In other words, development of the applied DFT methodology only became notable after Kohn W. and Sham L.J. released their reputable series of equations which are introduced as Kohn–Sham (KS) equations [38–43]. Considering the electronic density within the KS image directs us to a remarkable reduction of quantum computing. Thus, the KS methodology lightens the route for pursuing systems that cannot be discussed by conventional ab-initio methodologies. Kohn and Sham introduces the solution which brings up the mono-electronic orbitals to account the kinetic energy in a simple and relatively exact, by finding a residual modification that might be computed apart [42, 43]. Therefore, the precise exchange energy functional is described by the KS orbitals in lieu of the density which is cited as the indirect density functional. This research has employed the penetration of the hybrid functional of three-parameter basis set of B3LYP (Becke, Lee, Yang, Parr) within the conception of DFT upon theoretical computations [44–51].

In this article, the rigid PES using DFT calculations have been computed applying Gaussian 16 revision C.01 software [52]. The input Z-matrix for adsorption of CO molecules in air by the TM–B_4N_{10} has been designed with GaussView 6.1 [53] using 6-311+G(*d*, *p*), EPR-3, LANL2DZ basis set. In this study, the interaction between gas molecules and TM–B_4N_{10} was modeled and analyzed. As revealed by DFT-based analysis, the potency of TM–B_4N_{10} for grabbing CO molecules was determined mainly by the electronegativity of the functional groups, as well as the interaction between the TM–B_4N_{10} and CO molecules.

RESULTS AND DISCUSSION

One of the most dominant gas pollutants in the air is carbon monoxide. The data has evaluated the efficiency of boron nitride nanocage doped with Ti, V, Cr for gas detection. In fact, it can be remarked the chemisorptive nature of the bond among the gas molecules with boron and nitrogen elements through the equilibrium distribution of doping atoms, B_5N_{10}, and a monolayer attribute.

Projected Density of State and Electronic Evaluating

The electronic structures of CO adsorption on pristine B_5N_{10} and TM-doped B_5N_{10} as the selective sensor for detecting and grabbing gas molecules in the air have been illustrated using CAM–B3LYP–D3/6-311+G(*d*, *p*), LANL2DZ level of theory. Figure 2 shows the projected density of state (PDOS) of

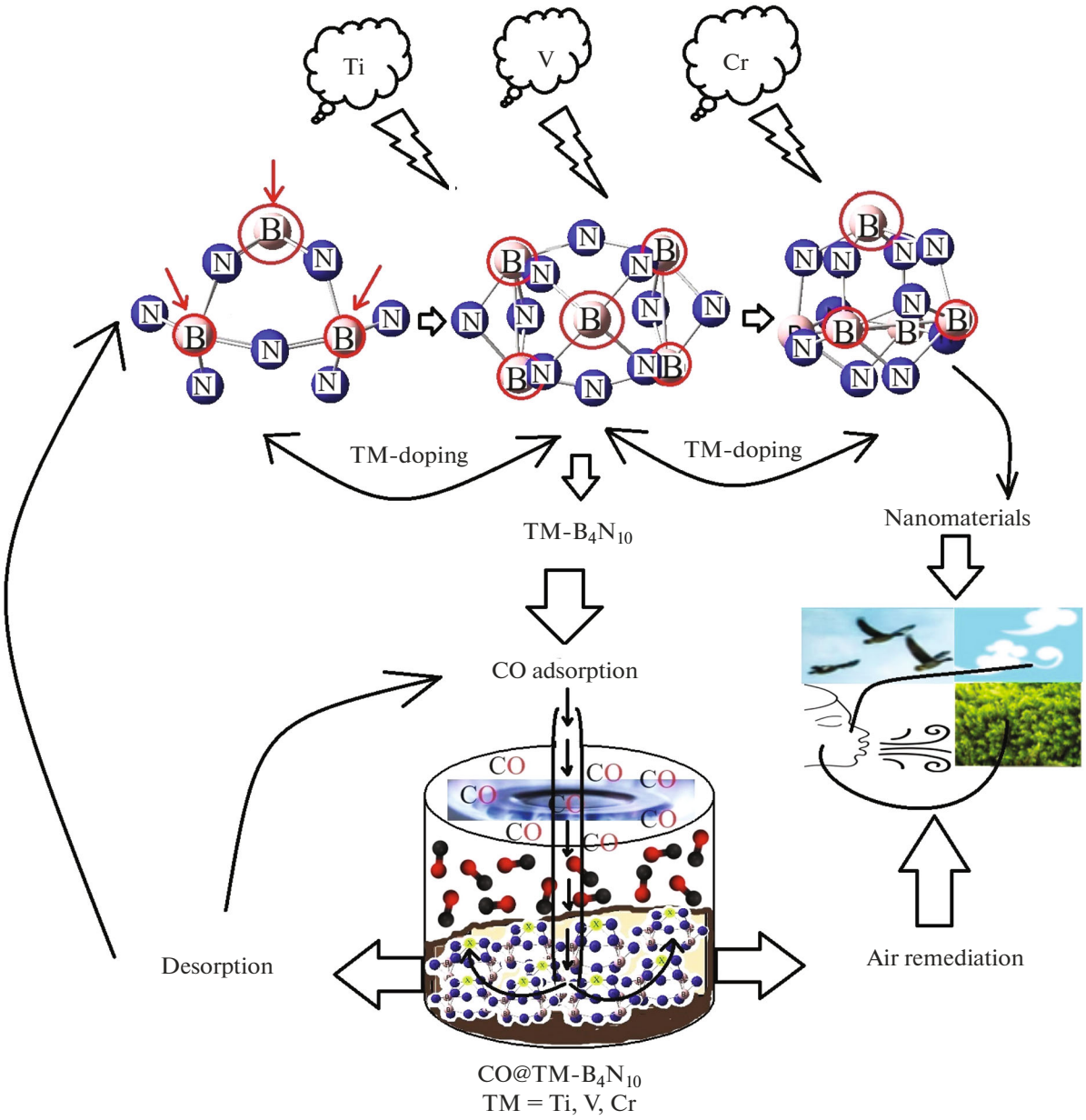

Fig. 1. Application of TM–B_4N_{10} towards adsorption of gas molecules of CO and formation of complexes: CO@Ti–B_4N_{10}, CO@V–B_4N_{10}, CO@Cr–B_4N_{10} complexes using CAM–B3LYP–D3/6-311+G(*d*, *p*), LANL2DZ calculation. (Note: the sign of adsorption is shown with @).

$CO@B_5N_{10}$ and CO@TM–B_4N_{10} through gas molecules adsorption. The appearance of the energy states (*p*-orbital) of C, N, O and (*d*-orbital) of Ti, V, Cr within the gap of TM–B_4N_{10} induces the reactivity of the system. It is clear from the figure that after trapping with gas molecules, there is a significant contribution of *d*-orbital in the unoccupied level. Therefore, the curve of partial PDOS has described that the *p* states of N atoms in gas molecules and *d*-orbital in Ti, V, Cr transition metals in TM–B_4N_{10} overcome due to the conduction band (Fig. 2). A distinguished adsorption trait might be seen in CO@TM–B_4N_{10} because of the potent interaction between the *p* states of carbon atom in gas molecules with *d* states of Ti, V, Cr in TM–B_4N_{10} complexes.

Figure 2 shows that $CO@B_5N_{10}$, CO@Ti –B_4N_{10}, CO@V–B_4N_{10}, CO@Cr–B_4N_{10} complexes through gas molecules adsorption, respectively, have the most

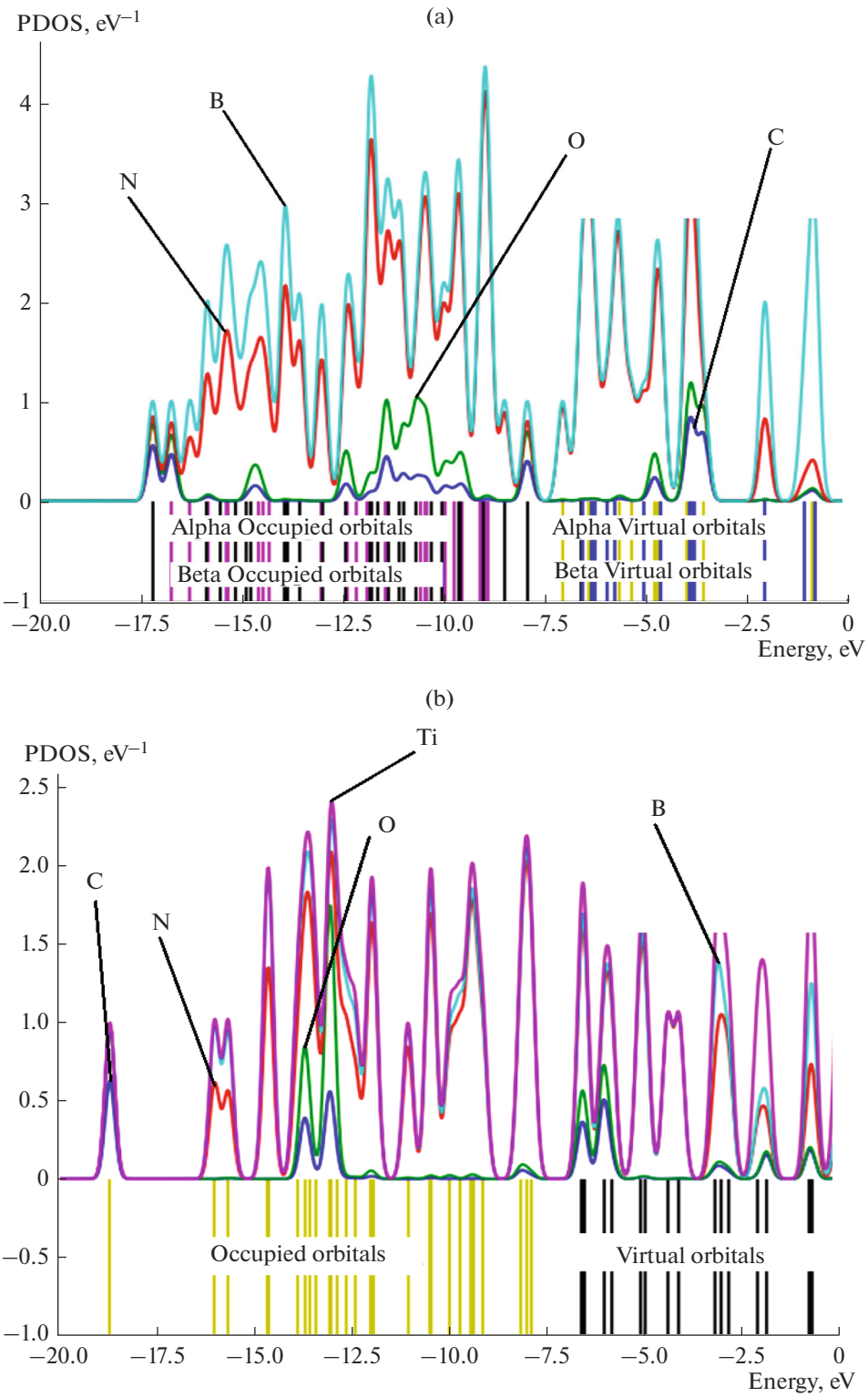

Fig. 2. PDOS of gas molecules of CO adsorbed on pristine B_5N_{10} and TM–B_4N_{10} including (a) CO@B_4N_{10}, (b) CO@Ti –B_4N_{10}, (c) CO@ V–B_4N_{10}, and (d) CO@ Cr–B_4N_{10} complexes by CAM–B3LYP–D3/6-311+G(*d*, *p*), LANL2DZ.

contribution at the middle of the conduction band between –5 to –15 eV, while contribution of boron and nitrogen states are enlarged and similar together, and adsorbing of CO depicts interfacial electronic of the B_5N_{10} for selection of this gas. CO@B_5N_{10} has indicated two sharp peak around –9 and –12.5 eV for B in

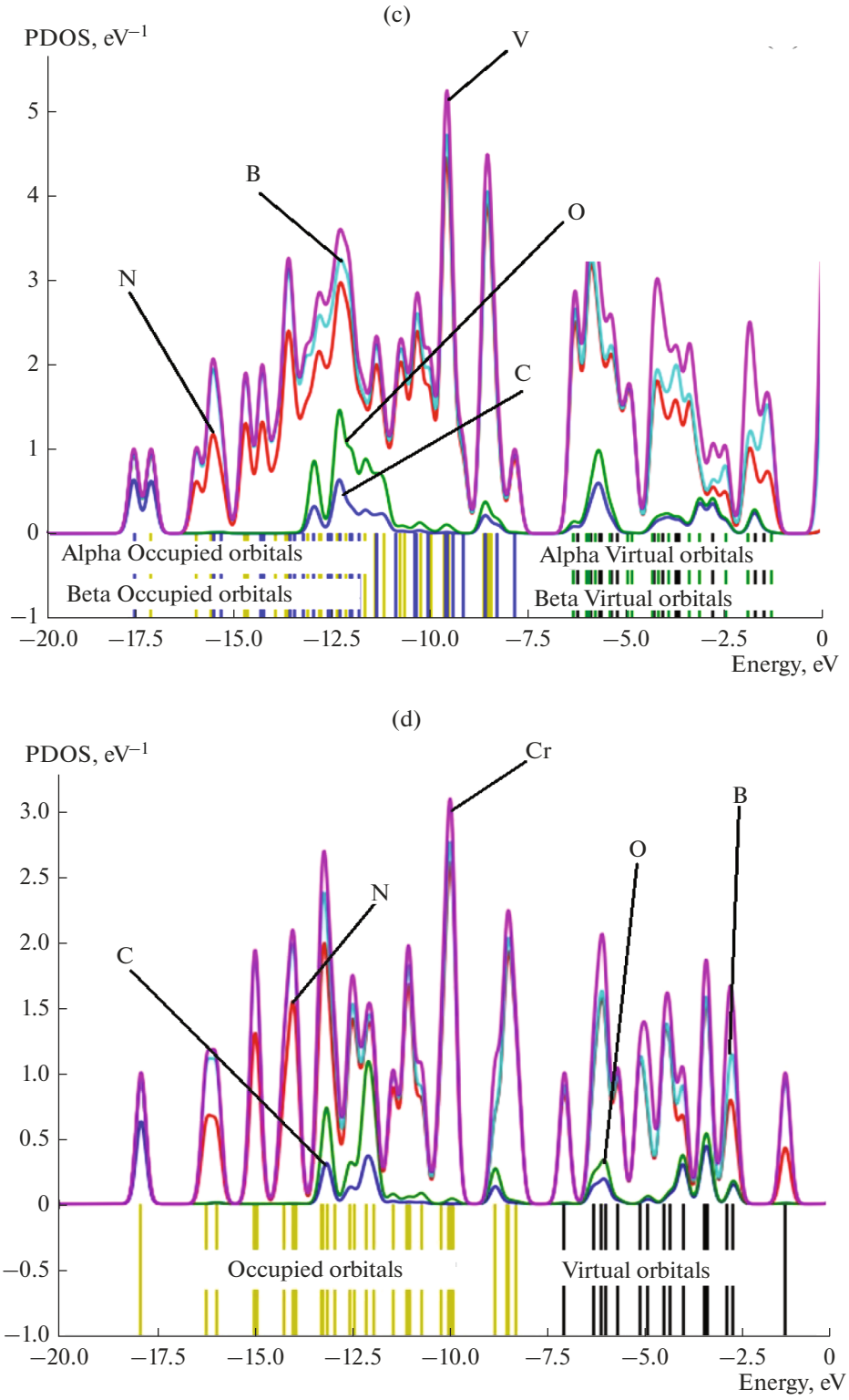

Fig. 2. (Contd.)

Fig. 2a, while CO@Ti $-B_4N_{10}$ has indicated one sharp peak around -12.5 eV for Ti in Fig. 2b, CO@V$-B_4N_{10}$ (Fig. 2c) and CO@Cr$-B_4N_{10}$ complexes (Fig. 2d) have exhibited two sharp peaks around -10 eV for V and Cr atoms, respectively. Therefore, the order potency of gas adsorption by doping atoms of Ti, V, Cr

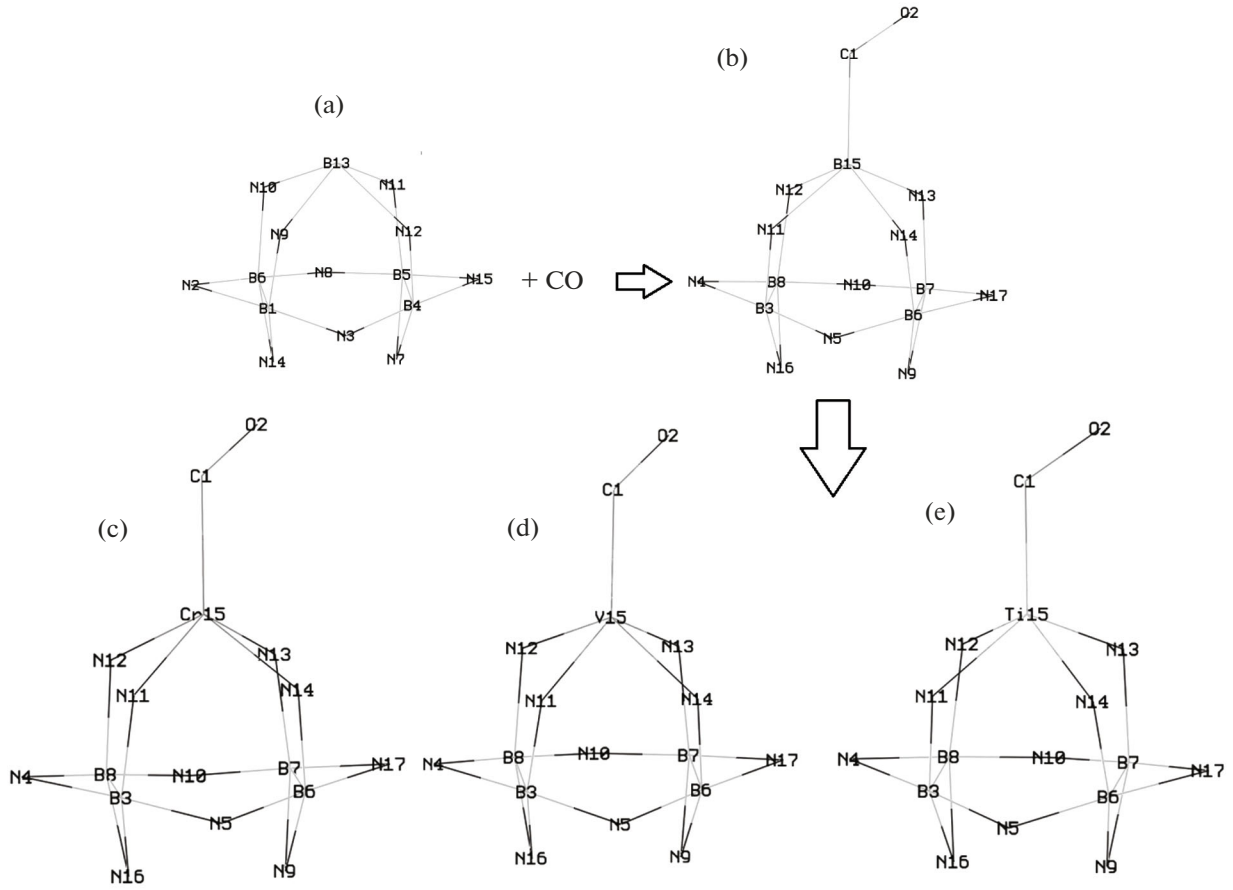

Fig. 3. Optimized structures of CO adsorbed on the surface of (a) pristine B_4N_{10} and formation of (b) CO@B_5N_{10} and TM–B_4N_{10} (TM = Ti, V, Cr) towards (c) CO@Ti–B_4N_{10}, (d) CO@V–B_4N_{10}, and (e) CO@Cr–B_4N_{10} complexes.

on B_5N_{10} based on the PDOS might be shifted as: Ti–B_4N_{10} > Cr–B_4N_{10} ≈ V–B_4N_{10} > B_5N_{10}.

Insight to Nuclear Quadrupole Resonance

Since the electric field gradient (EFG) at the citation of the nucleus in CO is allocated by the valence electrons twisted in the attachment with close nuclei of TM–B_4N_{10} through trapping of gas molecules (Fig. 3), the nuclear quadrupole resonance (NQR) frequency at which transitions occur is particular for CO@TM–B_4N_{10} complexes (Table 1) [54–57]. In this research work, the electric potential as the quantity of work energy through carrying over the electric charge from one position to another position in the essence of electric field has been evaluated for CO@ Ti –B_4N_{10}, CO@V–B_4N_{10}, and CO@Cr–B_4N_{10} complexes (Table 1).

In Table 1, the Bader charge and electronic potential properties of Ti, V, C and B, N in TM– B_4N_{10} and C, O of CO molecules trapped on doped-boron nitride nanocages have been investigated. The amounts indicate that with increasing the negative charge of different atoms, the electric potential resulted from NQR calculations increase. Moreover, the doping atoms of Ti(15), V(15), Cr(15) on the B_5N_{10} have shown the most potential for accepting the electron from electron donor of C(1) and O(2) in CO adsorbed on the TM–B_4N_{10} (Table 1).

Furthermore, in Fig. 4, it has been sketched the electric potential of nuclear quadrupole resonance for some atoms of B, N/Ti, V, Cr in pristine B_5N_{10},TM–B_4N_{10} and C, O of gas molecules trapped on doped-boron nitride nanocages which has been calculated by CAM–B3LYP–D3/EPR-3, LANL2DZ. Figure 4a with R^2 = 0.9209 has indicated the fluctuation of istropic and anisotropic chemical shift for pristine B_5N_{10}. In Figs. 4b and 4c, it was observed the behavior of CO adsorption on the Ti–B_4N_{10} and CO@V–B_4N_{10}, with the analogous high sensitivity based on relation coefficient of R^2 = 0.986 and R^2 = 0.9323, respectively. Adsorption of CO on the Cr–B_4N_{10} has illustrated the highest sensing of R^2 = 0.9666 (Fig. 4d).

It's vivid that the curve of TM–B_4N_{10} is waved by CO molecules. The fluctuated peaks for electric potential have been shown around CO trapping on the

Table 1. The electric potential (a.u.) and Bader charge (e) through NQR calculation for CO@Ti–B_4N_{10}, CO@V–B_4N_{10}, and CO@Cr–B_4N_{10} complexes using CAM–B3LYP–D3/EPR-3, LANL2DZ calculation

$CO@B_5N_{10}$			$CO@Ti-B_4N_{10}$		
atom	Q	E_p	atom	Q	E_p
C1	0.1563	−14.5993	C1	0.1679	−14.5375
O2	−0.2426	−22.2602	O2	−0.1297	−22.1646
B3	0.1261	−11.264	B3	0.1532	−11.2825
N4	−0.0253	−18.2617	N4	−0.0479	−18.2904
N5	−0.0590	−18.2439	N5	-0.0562	−18.2724
B6	0.1284	−11.2639	B6	0.1410	−11.2804
B7	0.1275	−11.2644	B7	0.1480	−11.2816
B8	0.1290	−11.2642	B8	0.1419	−11.2804
N9	−0.0761	−18.2534	N9	−0.0585	−18.2696
N10	−0.0596	−18.2443	N10	−0.0530	−18.2715
N11	−0.0932	−18.2515	N11	−0.2665	−18.2967
N12	−0.0920	−18.2515	N12	−0.2622	−18.2899
N13	−0.0725	−18.2517	N13	−0.2641	−18.297
N14	−0.0942	−18.2512	N14	−0.2600	−18.2899
B15	0.2448	−11.2133	Ti15	0.7499	−10.8373
N16	−0.0753	−18.2534	N16	−0.0615	−18.2726
N17	−0.0224	−18.2617	N17	−0.0423	−18.2889
$CO@V-B_4N_{10}$			$CO@Cr-B_4N_{10}$		
atom	Q	E_p	atom	Q	E_p
C1	0.0671	−14.5865	C1	0.1019	−14.5703
O2	−0.1799	−22.2083	O2	−0.2053	−22.2094
B3	0.1170	−11.2803	B3	0.1285	−11.271
N4	−0.0334	−18.2771	N4	−0.0515	−18.2755
N5	−0.0760	−18.28	N5	−0.0936	−18.2746
B6	0.1205	−11.2795	B6	0.1442	−11.2733
B7	0.1114	−11.28	B7	0.1227	−11.2688
B8	0.1162	−11.2789	B8	0.1439	−11.2743
N9	−0.0357	−18.2707	N9	−0.0452	−18.2605
N10	−0.0718	−18.2783	N10	−0.0936	−18.2754
N11	−0.1883	−18.2792	N11	−0.1418	−18.2607
N12	−0.1888	−18.2783	N12	−0.1738	−18.2605
N13	−0.1862	−18.2803	N13	−0.1517	−18.2623
N14	−0.1924	−18.279	N14	−0.1728	−18.2598
V15	0.6893	−12.535	Cr15	0.5883	−14.3983
N16	−0.0362	−18.2701	N16	−0.0518	−18.2647
N17	−0.0330	−18.2773	N17	−0.0483	−18.2739

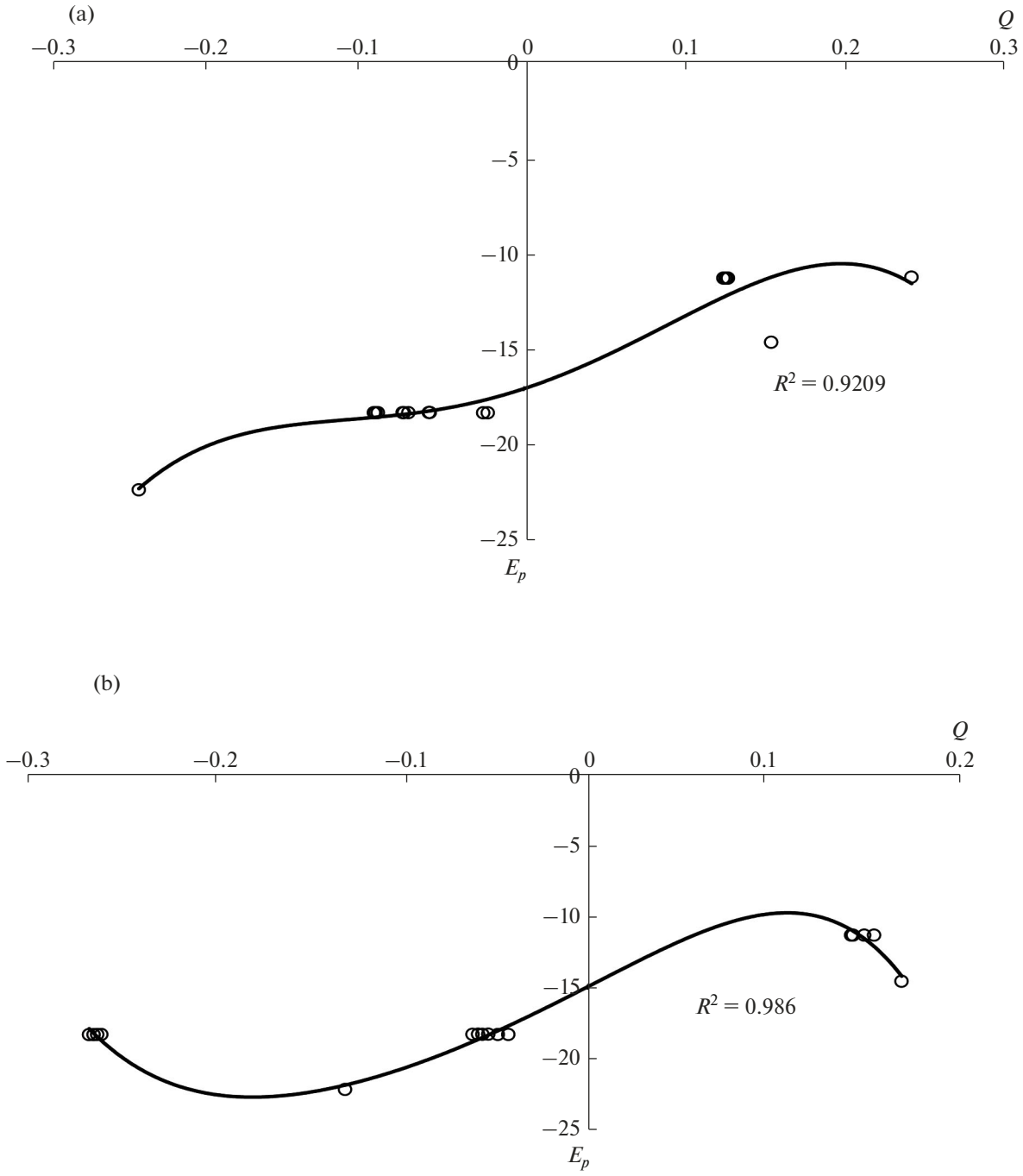

Fig. 4. Electric potential (E_p/a.u.) versus Bader charge (Q/coulomb) through NQR calculation for (a) CO@B_5N_{10} (b) CO@Ti – B_4N_{10}, (c) CO@V–B_4N_{10}, and (d) CO@Cr–B_4N_{10} complexes by CAM–B3LYP–D3/EPR-3, LANL2DZ.

TM–B_4N_{10} which demonstrates the electron accepting specifications of carbon and oxygen versus the titanium, vanadium, and chromium doped on the B_4N_{10} (Fig. 4). Besides, it can be considered that transitions metals as ferromagnetic semiconductors in the functionalized B_5N_{10} might have more impressive sensitivity for accepting the electrons from CO by Ti, V, Cr in the process of adsorption mechanism. Table 1 has shown that the adsorbents of chromium with 0.5883, vanadium with 0.6893, and titanium with 0.7499 coulomb, respectively, have presented the most tendency for being the electron acceptors. In fact, the uptake of gas molecules has been known to be associated with TM–B_4N_{10}, indicating that the adsorbed CO molecules in the TM–doped nanocage can be internalized through a different pathway from pristine B_5N_{10} nanocage.

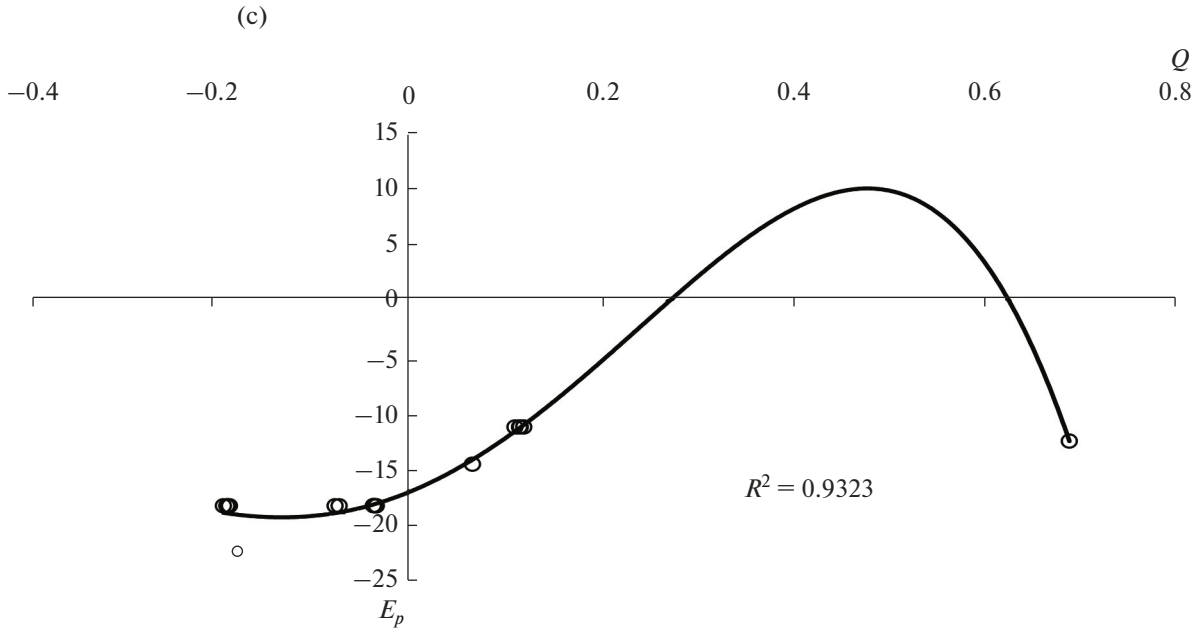

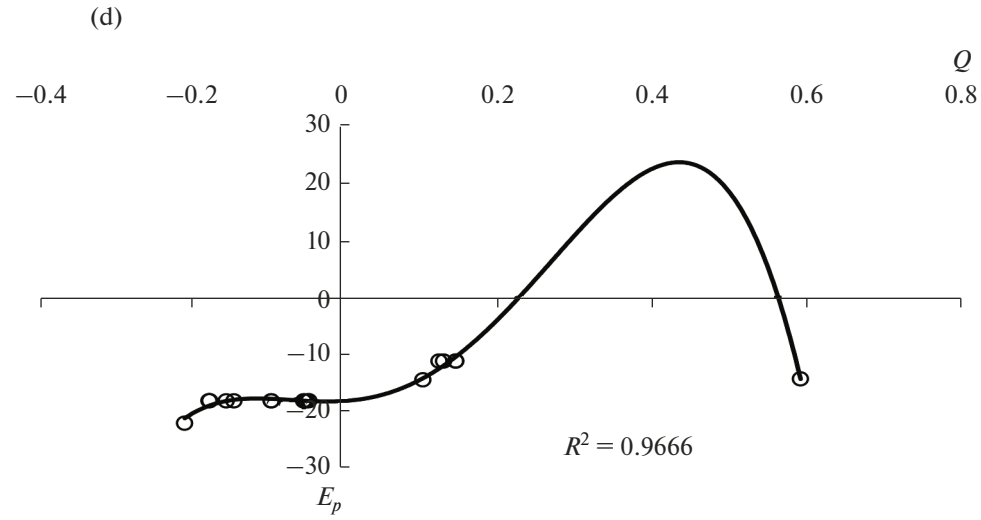

Fig. 4. (Contd.)

Analysis of Nuclear Magnetic Resonance Spectra

Based on resulted amounts, nuclear magnetic resonance (NMR) spectra of TM–B_4N_{10} as the potent sensor for adsorbing toxic gas molecules of CO can unravel the efficiency of TM–B_4N_{10} for detecting and removing of these hazardous gases in air as an ecofriendly approach. From the DFT calculations, it has been attained the chemical shielding (CS) tensors in the principal axes system to estimate the isotropic chemical-shielding (CSI) and anisotropic chemical-shielding (CSA) [58–68].

The NMR data of isotropic (σ_{iso}) and anisotropic shielding tensors (σ_{aniso}) of gas molecules trapped in the pristine B_5N_{10} nanocage and TM–B_4N_{10} towards formation of CO@B_5N_{10}, CO@Ti–B_4N_{10}, CO@V–B_4N_{10}, and CO@Cr–B_4N_{10} complexes have been computed by Gaussian 16 revision C.01 program package [52] and been shown in Table 2. In Table 2, NMR data has reported the notable amounts for CO

Table 2. Data of NMR shielding tensors for selected atoms of CO@Ti–B_4N_{10}, CO@V–B_4N_{10}, and CO@Cr–B_4N_{10} complexes using CAM–B3LYP–D3/6-311+G(*d*, *p*), LANL2DZ calculation

$CO@B_5N_{10}$			$CO@Ti–B_4N_{10}$		
atom	σ_{iso}	σ_{aniso}	atom	σ_{iso}	σ_{aniso}
C1	251.2150	186.5434	C1	388.8511	666.7627
O2	883.0962	162.3406	O2	1283.8732	1685.3315
B3	69.1160	72.2321	B3	117.2886	102.8982
N4	885.9787	979.9144	N4	891.6795	12840.5030
N5	144.4949	316.8495	N5	2581.3254	13809.2948
B6	69.4908	71.9415	B6	85.0063	73.4353
B7	68.8569	71.8869	B7	113.4469	184.3166
B8	69.3353	71.4020	B8	100.3561	104.0940
N9	269.5921	650.8331	N9	2515.2774	4029.0751
N10	164.9927	340.0788	N10	1147.6386	15164.8980
N11	750.5269	266.0050	N11	1403.4501	2850.4956
N12	735.6351	293.0488	N12	1553.1439	3084.0244
N13	758.8548	272.9724	N13	848.1172	2567.4336
N14	731.6272	299.9218	N14	706.4805	2271.1598
B15	109.8284	23.6772	Ti15	1187.2260	1138.4861
N16	266.2934	659.9829	N16	290.9426	5510.7548
N17	883.9536	998.7297	N17	3332.5747	7753.1427
$CO@V–B_4N_{10}$			$CO@Cr–B_4N_{10}$		
atom	σ_{iso}	σ_{aniso}	atom	σ_{iso}	σ_{aniso}
C1	260.9712	393.3751	C1	292.1782	694.1805
O2	735.9242	1104.0681	O2	633.1859	3188.7465
B3	70.3244	66.7736	B3	39.2967	99.6046
N4	1177.9192	1203.5066	N4	1870.028	2661.9993
N5	819.5890	610.2603	N5	131.5764	2171.5379
B6	70.5210	67.1702	B6	52.5392	46.2836
B7	70.2874	67.7906	B7	38.0691	111.9754
B8	70.3698	67.5527	B8	54.2128	45.9159
N9	109.5248	931.7893	N9	378.9198	1752.4055
N10	784.4759	495.8301	N10	928.6784	2162.4106
N11	598.2535	722.0654	N11	813.3494	2124.0132
N12	609.7100	892.8854	N12	70.9784	2292.9194
N13	560.6195	750.5350	N13	1115.886	2122.6552
N14	540.1301	766.4368	N14	147.3939	1954.1015
V15	4008.2481	478.9168	Cr15	12676.227	4962.3842
N16	94.5760	753.2783	N16	14.0527	1720.0787
N17	1248.6618	1250.0664	N17	1283.8952	4581.8198

which were adsorbed on the pristine B_5N_{10} nanocage and TM–B_4N_{10} as the selective sensor for detecting gas molecules in the air. The observed increase in the chemical shift anisotropy spans for C(1) and O(2) atoms of CO adsorption on the TM–B_4N_{10}. The observed weak signal intensity near the parallel edge of the nanocage pattern may be due to boron binding induced non-spherical distribution of these complexes.

It is remarkable that doping of Ti, V, Cr on B_4N_{10} might promote the stability of nanocage that results in

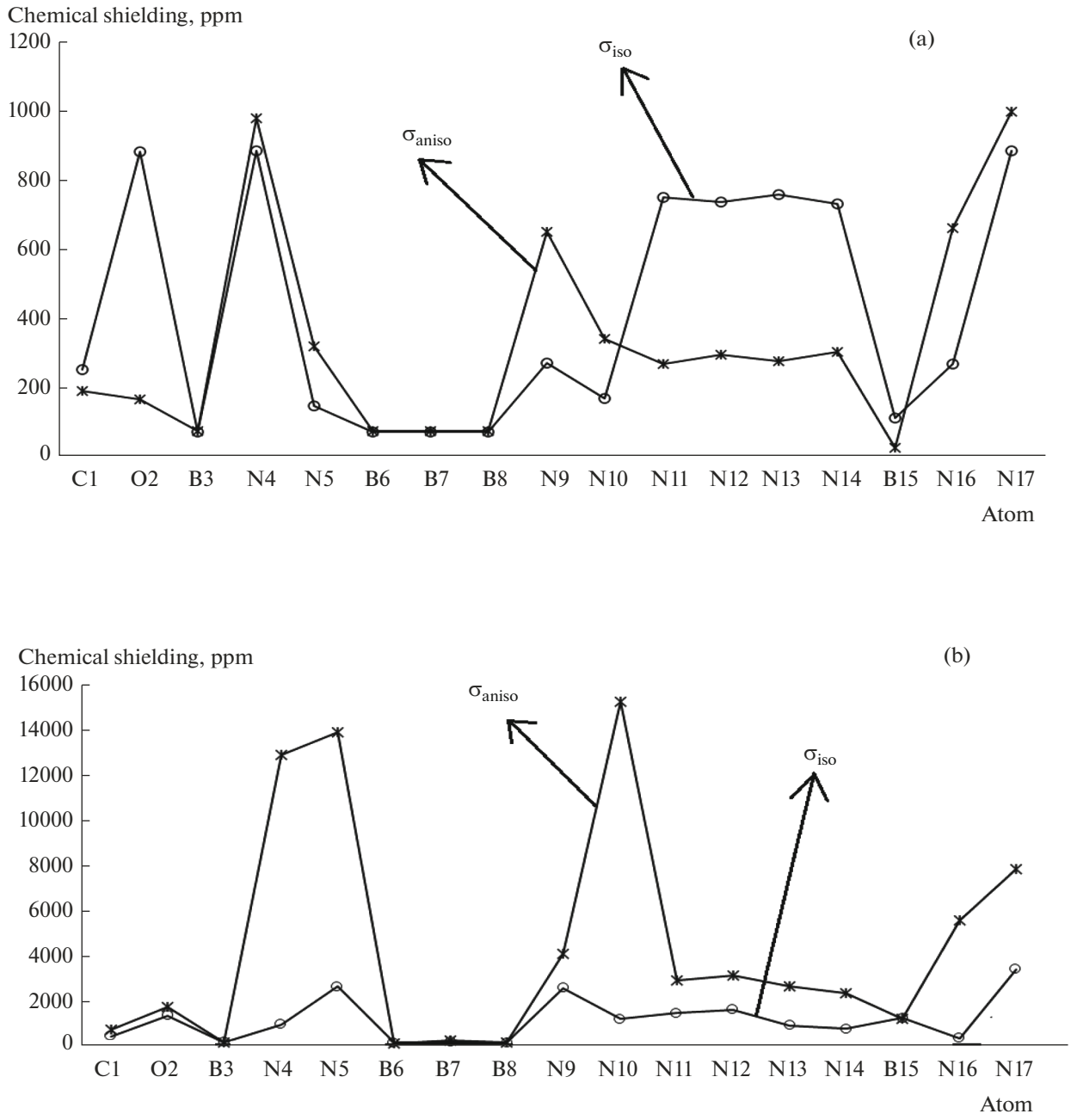

Fig. 5. The NMR spectra for (a) CO@B_5N_{10}, (b) CO@Ti–B_4N_{10}, (c) CO@V–B_4N_{10}, and (d) CO@Cr–B_4N_{10} complexes using CAM–B3LYP–D3/6-311+G(*d*, *p*), LANL2DZ.

enhanced magnetic alignment of complexes. Interestingly, the reported results show that Ti, V, Cr elements can be optimized to achieve optimal alignment of nanocage in the presence of an applied magnetic field. In fact, the adsorption of CO can introduce spin polarization on the TM–B_4N_{10} which indicates that these surfaces might be applied as magnetic scavenging surface as a gas detector. Isotropic and anisotropic shielding fluctuate with the occupancy in the electron accepting gas molecules trapped in the atom-doped on the boron nitride nanocage.

Figure 5 exhibited the same tendency of shielding for boron and nitrogen; however, a considerable deviation exists from doping atoms of Ti(15), V(15), Cr(15) through interaction with C(1) and O(2) of CO during adsorbing on the pristine B_5N_{10} nanocage. In Fig. 5, gas molecules of CO in the complexes of CO@B_5N_{10} (Fig. 5a), CO@Ti–B_4N_{10} (Fig. 5b), CO@V–B_4N_{10} (Fig. 5c), and CO@Cr–B_4N_{10} (Fig. d) denote the fluctuation in the chemical shielding during gas trapping. Figures 5b–5d shows the gap

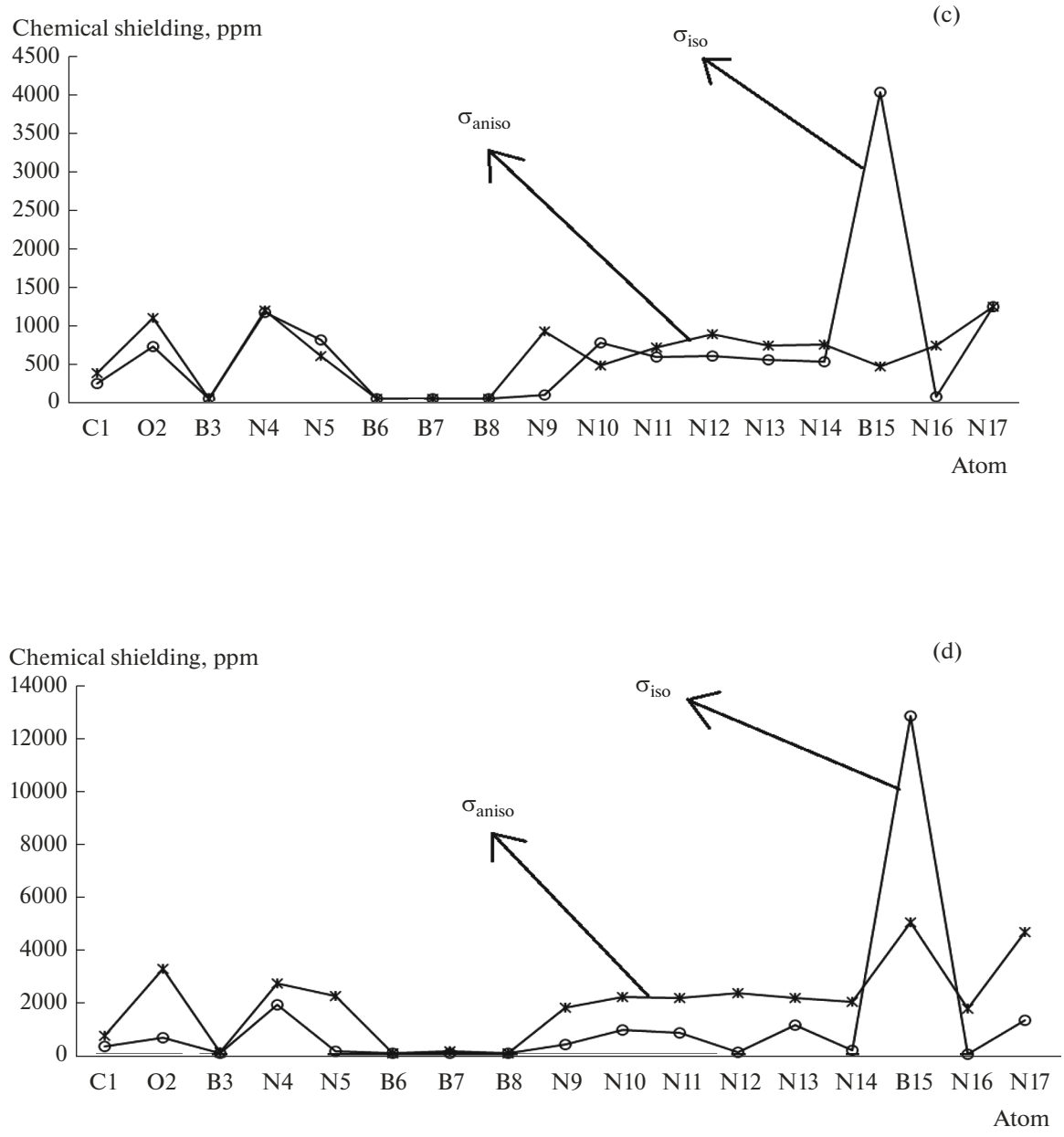

Fig. 5. (Contd.)

chemical shielding between titanium, vanadium, chromium doping of TM–B_4N_{10} nanocage and CO gas molecules. The yield of electron accepting for doping atoms on the TM–B_4N_{10} through gas molecules adsorption can be ordered as: Cr > V > Ti that approves the possibility of covalent bond between titanium, vanadium, chromium and carbon monoxide towards removing it from the air.

In the NMR spectroscopy, it has been observed the remarkable peaks around interaction of CO molecules through adsorbing on the TM–B_4N_{10} during toxic gas detection and its scavenging from the air; however, there are some fluctuations in the chemical shielding behaviors of isotropic and anisotropy attributes. Therefore, the authors believe that the extracted results would be useful in the design of TM–B_4N_{10} complexes based doped nanomaterials for increasing the adsorption of CO gas molecules in addition to the structural studies using solid-state and solution NMR techniques.

Infrared Spectroscopy and Thermodynamic Factors

The infrared (IR) calculations have been accomplished for adsorption of CO molecules by pristine

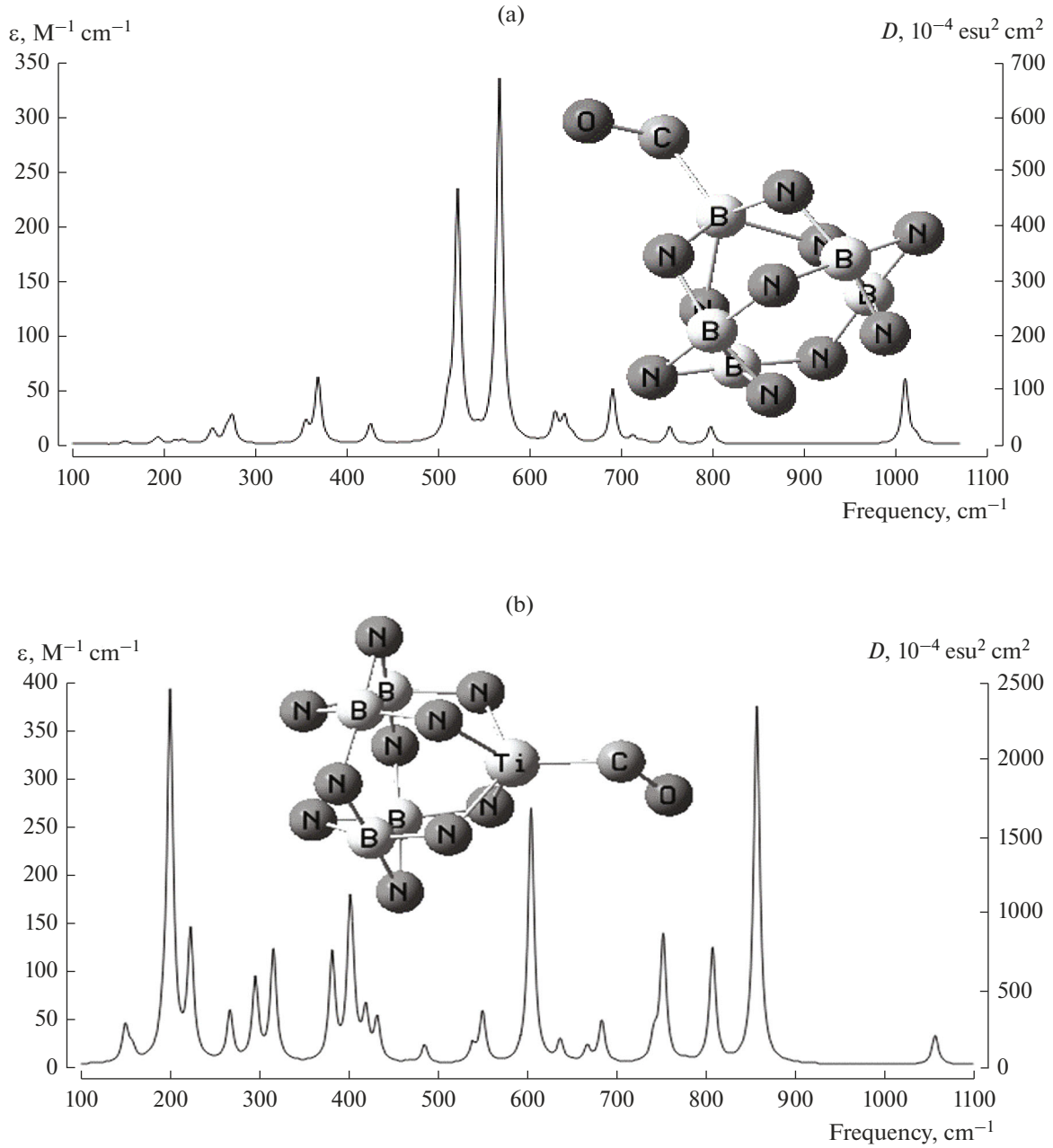

Fig. 6. The Frequency (cm^{-1}) changes through the IR spectra for (a) CO@B_5N_{10}, (b) CO@Ti–B_4N_{10}, (c) CO@V–B_4N_{10}, and (d) CO@Cr–B_4N_{10} complexes using CAM–B3LYP–D3/6-311+G(*d*, *p*), LANL2DZ [*Note*: ε (M^{-1} cm^{-1}) is the absorbance unit and D (10^{-4} esu^2 cm^2) is the dipole strength via the esu or electrostatic unit, which is a unit of charge in the cgs (centimeter-gram-second system)].

B_5N_{10} nanocage and TM–B_4N_{10} during toxic gas sensing in air. Therefore, it has been simulated the several clusters containing CO@B_5N_{10} (Fig. 6a), CO@Ti–B_4N_{10} (Fig. 6b), CO@V–B_4N_{10} (Fig. 6c), and CO@Cr–B_4N_{10} (Fig. 6d) complexes using CAM–B3LYP–D3/6-311+G(*d*, *p*), LANL2DZ at 300 K. The graph of Fig. 6a has been seen in the frequency range between 100–1100 cm^{-1} for CO@B_5N_{10} with two sharp peaks around 520.63 and 566.41 cm^{-1}. The curve of Fig. 6b has been observed in the frequency range between 100–1100 cm^{-1} for CO@Ti –B_4N_{10} with sharp peaks around 202.69, 606.23 and 858.53 cm^{-1}. Figure 6c has shown the frequency range between 100–1100 cm^{-1} for CO@V–B_4N_{10} with sharp peaks around 369.36, 422.65 and 603.26 cm^{-1}. Figure 6d has indicated the fluctuation of frequency between 100–1100 cm^{-1} for CO@Cr–B_4N_{10} with several sharp peaks around 328.93, 433.18 and 554.91 cm^{-1}.

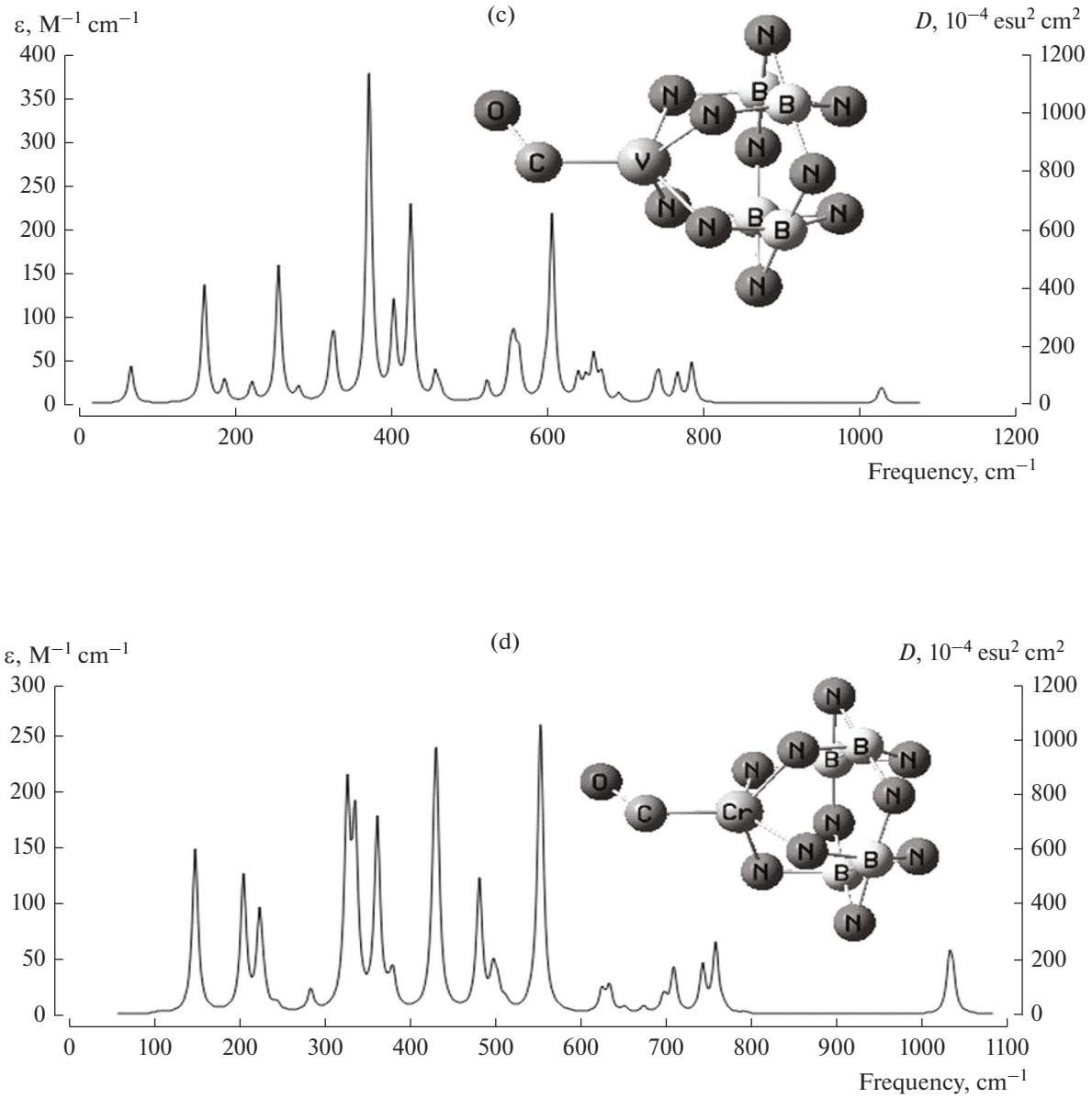

Fig. 6. (Contd.)

The IR spectra of CO adsorption on the TM–B_4N_{10} has demonstrated that the structure of the dominant complex correlates with the electron potency of TM-doped on the pristine B_5N_{10} nanocage. As it has been seen the doped nanocages of Ti–B_4N_{10}, V–B_4N_{10}, and Cr–B_4N_{10} complexes have the most fluctuations and the highest tendency for adsorption of CO around 450 cm^{-1}. Therefore, it can be found that IR spectroscopy of CO-adsorbed TM–B_4N_{10} is now well-placed to address specific questions on the individual effect of charge carriers (gas molecule-nanocage), as well as doping atoms on the overall structure (Figs. 6b–6d).

Table 3 through the thermodynamic specifications concluded that TM–B_4N_{10} due to adsorption of CO might be more efficient sensors than pristine B_5N_{10} nanocage for detecting and removing the gas molecules from the polluted air. Thermodynamic parameters of CO gas molecules adsorption on the TM–B_4N_{10} have been determined using DFT theoretical technique at 300 K. It has been shown that for a given number of carbon donor sites in CO, the stabilities of complexes owing to doping atoms of Ti, V, Cr can be considered as: CO@Cr–B_4N_{10} > CO@V–B_4N_{10} ⩾ CO@Ti –B_4N_{10} (Table 3). The curve in Fig. 7 could figure out the maximum efficiency of Ti, V, Cr atoms doping of B_5N_{10} for gas molecules adsorption through

Table 3. The thermodynamic characters of CO@Ti–B_4N_{10}, CO@V–B_4N_{10}, and CO@Cr–B_4N_{10} complexes using CAM–B3LYP–D3/6-311+G(*d*, *p*), LANL2DZ calculation at 300 K

Compound	$\Delta E^o \times 10^{-3}$, kcal/mol	$\Delta H^o \times 10^{-3}$, kcal/mol	$\Delta G^o \times 10^{-3}$, kcal/mol	S^o, cal/K mol	Dipole moment, Debye
B_5N_{10}	–420.550	–420.549	–420.579	100.650	0.2020
CO@B_5N_{10}	–491.651	–491.650	–491.681	103.336	3.1717
CO@Ti–B_4N_{10}	–512.565	–512.564	–512.595	102.375	3.4889
CO@V–B_4N_{10}	–521.152	–521.152	–521.183	106.021	1.1206
CO@Cr–B_4N_{10}	–530.213	–530.213	–530.244	104.267	1.2359

ΔG^o_{ads} at 300 K which depends on the covalent bond between CO gas molecules and TM–B_4N_{10} as a potent sensor for air pollution removal. The adsorption process of CO gas molecules on the TM–B_4N_{10} is affirmed by the ΔG^o_{ads} quantities:

$$\Delta G^o_{ads} = \Delta G^o_{CO@TM-B_4N_{10}} - \left(\Delta G^o_{CO} + \Delta G^o_{TM-B_4N_{10}}\right),$$
$$TM = Ti, V, Cr.$$

Figure 7 shows the key role of doped atoms of Ti, V, Cr during interaction between the adsorbates of CO gas molecules as the electron donors and the adsor-

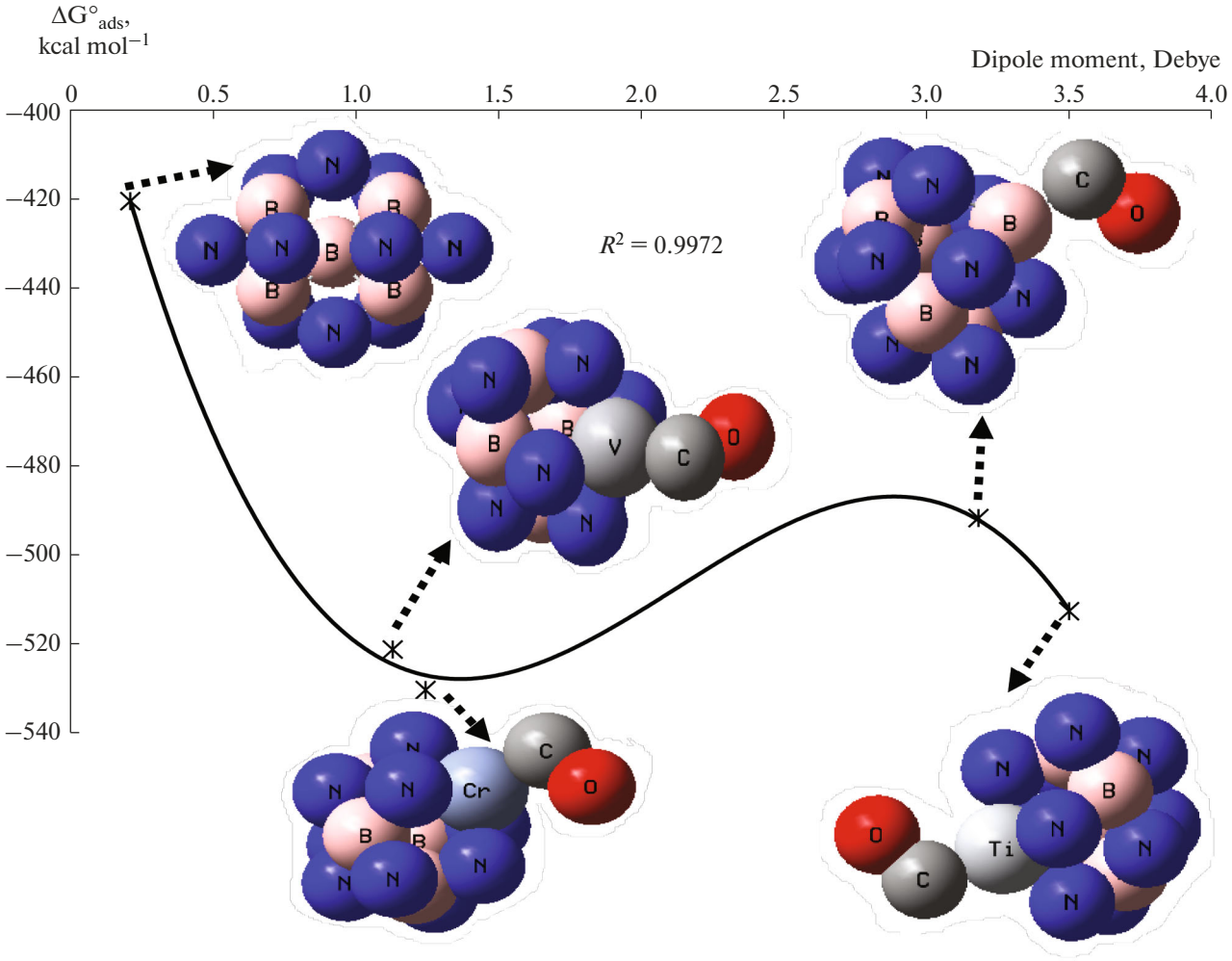

Fig. 7. The Gibbs free energy (ΔG^o_{ads}) versus dipole moment (Debye) for B_5N_{10}, CO@B_5N_{10}, CO@Ti–B_4N_{10}, CO@V–B_4N_{10}, and CO@Cr–B_4N_{10} complexes using CAM–B3LYP–D3/6-311+G(*d*, *p*), LANL2DZ calculation.

bent of Ti–B_4N_{10}, V–B_4N_{10}, and Cr–B_4N_{10} as electron acceptors. Therefore, the selectivity of atom-doped on boron nitride nanocage (gas sensor) for gas molecules adsorption can be resulted as: Cr > V > Ti (Table 3 and Fig. 7).

CONCLUSIONS

This research has investigated doping of Ti, V, Cr transition metals on the boron nitride nanocage (TM–B_4N_{10}) for enhancing toxic gas sensing of these nanomaterials for air pollution removal. Therefore, CO gas molecules separation involving the TM–B_4N_{10} has been experimented based on electrostatic interactions between the gas molecules and TM–B_4N_{10}.

The electromagnetic and thermodynamic properties of TM–B_4N_{10} complexes were computed using density functional theory at 300 K. The results have illustrated that chosen gas molecules adsorbed on the TM–B_4N_{10} are rather stable with the most stable adsorption site being in the center of TM–B_4N_{10} system. The selectivity of atom-doped on boron nitride nanocage (gas sensor) for gas molecules adsorption can be resulted as: CO@Cr–B_4N_{10} > CO@V–B_4N_{10} > CO@Ti–B_4N_{10}, respectively. This work proposes that transition metals as ferromagnetic semiconductors can be examined through doping on the nanomaterials for enhancing the adsorption potency towards designing the pollution removal sensors.

ACKNOWLEDGMENTS

In successfully completing this paper and its research, the authors are grateful to Kastamonu University.

FUNDING

This work was supported by ongoing institutional funding. No additional grants to carry out or direct this particular research were obtained.

CONFLICT OF INTEREST

The authors of this work declare that they have no conflicts of interest.

REFERENCES

1. D. Mayilyan and A. Aleksanyan, Russ. J. Phys. Chem. B **17**, 1177–1182 (2023). https://doi.org/10.1134/S199079312305007X
2. V. E. Kirillov, G. Y. Yurkov, M. S. Korobov, et al., Russ. J. Phys. Chem. B **17**, 1346–1354 (2023). https://doi.org/10.1134/S1990793123060040
3. G. V. Simbirtseva and S. D. Babenko, Russ. J. Phys. Chem. B **17**, 1309–1310 (2023). https://doi.org/10.1134/S1990793123060222
4. E. I. Rudenko, N. V. Dohlikova, A. K. Gatin, et al., Russ. J. Phys. Chem. B **17**, 845–852 (2023). https://doi.org/10.1134/S1990793123040164
5. F. Mollaamin and M. Monajjemi, Sensor Rev. **44** (2), 179–193 (2024). https://doi.org/10.1108/SR-01-2024-0066
6. F. Mollaamin, S. Mohammadi, Z. Khalaj, et al., Russ. J. Phys. Chem. B **18** (1), 67–82(2024). https://doi.org/10.1134/S1990793124010330
7. D. V. Shtansky, A. T. Matveev, E. S. Permyakova, et al., Nanomaterials **12**, 2810 (2022). https://doi.org/10.3390/nano12162810
8. Y. Yang, Y. Peng, M. F. Saleem, et al., Materials **15**, 4396 (2022). https://doi.org/10.3390/ma15134396
9. E. A. Lebedeva, S. A. Astaf'eva, and T. S. Istomina, Russ. J. Phys. Chem. B **16**, 316–322 (2022). https://doi.org/10.1134/S1990793122010109
10. R. S. Bangari, V. K. Yadav, J. K. Singh, et al., ACS Omega **5** (18), 10301–10314 (2020). https://doi.org/10.1021/acsomega.9b04295
11. Y. H. Chao, J. Zhang, H. P. Li, P. W. Wu, et al., Chem. Eng. J. **387**, 124138 (2020). https://doi.org/10.1016/j.cej.2020.124138
12. X.-Y. Lou, L. Yohai, and R. Boada, Molecules **29**, 59 (2024). https://doi.org/10.3390/molecules29010059
13. V. M. Solyanikov and L. V. Petrov, Russ. J. Phys. Chem. B **17**, 1259–1264 (2023). https://doi.org/10.1134/S1990793123060234
14. Y. Guo, R. X. Wang, P. F. Wang, et al., ACS Sustainable Chem. Eng. **7** (6), 5727–5741 (2019).
15. F. Mollaamin and M. Monajjemi, Sensor Rev. **43**, 266–279 (2023). https://doi.org/10.1108/SR-03-2023-0040
16. I. A. Palamarchuk, N. A. Gorshkova, O. S. Brovko, et al., Russ. J. Phys. Chem. B **17**, 1434–1441 (2023). https://doi.org/10.1134/S1990793123070096
17. F. Mollaamin and M. Monajjemi, J. Mol. Model. **29**, 170 (2023). https://doi.org/10.1007/s00894-023-05567-8
18. A. M. Aliev, G. K. Radzhabov, F. A. Vagabova, et al., Russ. J. Phys. Chem. B **17**, 1619–1627 (2023). https://doi.org/10.1134/S1990793123080067
19. F. Mollaamin and M. Monajjemi, Russ. J. Phys. Chem. B **18** (2), 533–548 (2024). https://doi.org/10.1134/S199079312402012X
20. A. Tahan, F. Mollaamin, and M. Monajjemi, Russ. J. Phys. Chem. **83**, 587–597 (2009). https://doi.org/10.1134/S003602440904013X
21. F. Mollaamin and M. Monajjemi, Russ. J. Phys. Chem. B **18** (2), 607–623 (2024). https://doi.org/10.1134/S1990793124020271
22. E. M. Sarasia, S. Afsharnezhad, B. Honarparvar, et al., Phys. Chem. Liq. **49**, 561–571 (2011). https://doi.org/10.1080/00319101003698992
23. F. Mollaamin and M. Monajjemi, Russ. J. Phys. Chem. B **18** (1), 49–66 (2024). https://doi.org/10.1134/S1990793124010159
24. M. Khaleghian, M. Zahmatkesh, F. Mollaamin, et al., Fullerenes, Nanotubes Carbon Nanostruct. **19**, 251–

261 (2011).
https://doi.org/10.1080/15363831003721757

25. F. Mollaamin, M. Monajjemi, S. Salemi, et al., Fullerenes, Nanotubes Carbon Nanostruct. **19**, 182 (2011).
https://doi.org/10.1080/15363831003782932
26. M. Monajjemi, M. Khaleghian, N. Tadayonpour, et al., Int. J. Nanosci. **09**, 517–529 (2010).
https://doi.org/10.1142/S0219581X10007071
27. F. Mollaamin and M. Monajjemi, J. Clust. Sci. **34**, 2901 (2023).
https://doi.org/10.1007/s10876-023-02436-5
28. F. Mollaamin and M. Monajjemi, Russ. J. Phys. Chem. B **17**, 658–672 (2023).
https://doi.org/10.1134/S1990793123030223
29. M. A. A. Zadeh, H. Lari, L. Kharghanian, et al., J. Comput. Theor. Nanosci. **12**, 4358 (2015).
https://doi.org/10.1166/jctn.2015.4366
30. M. Monajjemi, F. Mollaamin, and S. Shojaei, Biointerface Res. Appl. Chem. **10**, 5575 (2020).
https://doi.org/10.33263/BRIAC103.575585
31. S. Shahriari, F. Mollaamin, and M. Monajjemi, Micromachines **14**, 241 (2023).
https://doi.org/10.3390/mi14020241
32. F. Mollaamin, A. Ilkhani, N. Sakhaei, et al., J. Comput. Theor. Nanosci. **12**, 3148–3154 (2015).
https://doi.org/10.1166/jctn.2015.4092
33. M. Monajjemi, L. Mahdavian, F. Mollaamin, et al., Russ. J. Inorg. Chem. **54**, 1465–1473 (2009).
https://doi.org/10.1134/S0036023609090216
34. M. Monajjemi, M. T. Baie, and F. Mollaamin, Russ. Chem. Bull. **59**, 886–889 (2010).
https://doi.org/10.1007/s11172-010-0181-5
35. S. Shahriari, M. Monajjemi, and F. Mollaamin, J. Chil. Chem. Soc. **67**, 5468–5476 (2022).
https://doi.org/10.4067/S0717-97072022000205468
36. F Mollaamin and M. Monajjemi, J. Comput. Theor. Nanosci. **12**, 1030–1039 (2015).
https://doi.org/10.1166/jctn.2015.3846
37. M. M. Avilova, N. V. Zolotareva, and O. V. Popova, Russ. J. Phys. Chem. B **17**, 329–335 (2023).
https://doi.org/10.1134/S1990793123020203
38. V. B. Orel, and A. A. Manzhueva, Russ. J. Phys. Chem. B **17**, 835–844 (2023).
https://doi.org/10.1134/S1990793123040152
39. J. P. Perdew, K. Burke and M. Ernzerhof, Phys. Rev. Lett. **77**, 3865 (1996).
https://doi.org/10.1103/PhysRevLett.77.3865
40. X. Miao, S. Zhou, and C. Wang, Russ. J. Phys. Chem. B **16**, 804–808 (2022).
https://doi.org/10.1134/S199079312204011X
41. M. Arrigoni and G. K. H. Madsen, Comput. Mater. Sci. **156**, 354–360 (2019).
https://doi.org/10.1016/j.commatsci.2018.10.005
42. P. Hohenberg and W. Kohn, Phys. Rev. B **136**, B864–B871 (1964).
https://doi.org/10.1103/PhysRev.136.B864
43. W. Kohn and L. J. Sham, Phys. Rev. **140**, A1133–A1138 (1965).
https://doi.org/10.1103/PhysRev.140.A1133
44. A. D. Becke, J. Chem. Phys. **98**, 5648–5652 (1993).
https://doi.org/10.1063/1.464913
45. C. Lee, W. Yang, and R. G. Parr, Phys. Rev. B **37**, 785–789 (1988).
https://doi.org/10.1103/PhysRevB.37.785
46. K. Kim and K. D. Jordan, J. Phys. Chem. **98**, 10089–10094 (1994).
https://doi.org/10.1021/j100091a024
47. R. Alaya, K. Kourchid, Y. Althaqafi, et al., Russ. J. Phys. Chem. B **17**, 868–877 (2023).
https://doi.org/10.1134/S1990793123040024
48. C. J. Cramer, *Essentials of Computational Chemistry: Theories and Models*, 2nd ed. (Wiley, 2004).
49. F. Mollaamin and M. Monajjemi, J. Mol. Struct. **1300**, 137214 (2024).
https://doi.org/10.1016/j.molstruc.2023.137214
50. F. Mollaamin and M. Monajjemi, Mol. Simul. **49**, 365 (2023).
https://doi.org/10.1080/08927022.2022.2159996
51. E. A. Neskoromnaya, A. V. Babkin, E. A. Zakharchenko, et al., Russ. J. Phys. Chem. B **17**, 818–825 (2023).
https://doi.org/10.1134/S1990793123040139
52. M. J. Frisch, G. W. Trucks, H. B. Schlegel, G. E. Scuseria, M. A. Robb, J. R. Cheeseman, G. Scalmani, V. Barone, G. A. Petersson, H. Nakatsuji, X. Li, M. Caricato, A. V. Marenich, J. Bloino, B. G. Janesko, R. Gomperts, B. Mennucci, H. P. Hratchian, J. V. Ortiz, A. F. Izmaylov, J. L. Sonnenberg, D. Williams-Young, F. Ding, F. Lipparini, F. Egidi, J. Goings, B. Peng, A. Petrone, T. Henderson, D. Ranasinghe, V. G. Zakrzewski, J. Gao, N. Rega, G. Zheng, W. Liang, M. Hada, M. Ehara, K. Toyota, R. Fukuda, J. Hasegawa, M. Ishida, T. Nakajima, Y. Honda, O. Kitao, H. Nakai, T. Vreven, K. Throssell, J. A. Montgomery, Jr., J. E. Peralta, F. Ogliaro, M. J. Bearpark, J. J. Heyd, E. N. Brothers, K. N. Kudin, V. N. Staroverov, T. A. Keith, R. Kobayashi, J. Normand, K. Raghavachari, A. P. Rendell, J. C. Burant, S. S. Iyengar, J. Tomasi, M. Cossi, J. M. Millam, M. Klene, C. Adamo, R. Cammi, J. W. Ochterski, R. L. Martin, K. Morokuma, O. Farkas, J. B. Foresman, and D. J. Fox, Gaussian 16, Revision C.01, Gaussian, Inc., Wallingford CT, 2016.
53. R. Dennington, T. A. Keith, and J. M. Millam, GaussView, Version 6.06.16 (Semichem Inc., Shawnee Mission, KS, 2016).
54. A. H. Davtyan, Z. O. Manukyan, S. D. Arsentev, et al., Russ. J. Phys. Chem. B **17**, 336–345 (2023).
https://doi.org/10.1134/S1990793123020239
55. Z. Trontelj, J. Pirnat, V. Jazbinšek, et al., Crystals **10**, 450 (2020).
https://doi.org/10.3390/cryst10060450
56. O. Poleshchuk, E. Kalinina, J. Latosińska, et al., J. Mol. Struct. (Theochem.) **547**, 233–243 (2001).
https://doi.org/10.1016/S0166-1280(01)00636-4
57. O. Hotra and A. Samila, Electronics **9**, 1996 (2020).
https://doi.org/10.3390/electronics9121996
58. U. Sohail, F. Ullah, N. H. Binti Zainal Arfan, et al., Molecules **28**, 4060 (2023). .
https://doi.org/10.3390/molecules28104060

59. F. Mollaamin, S. Shahriari, M. Monajjemi, et al., J. Cluster Sci. **34**, 1547–1562 (2023). https://doi.org/10.1007/s10876-022-02335-1
60. B. Khalili Hadad, F. Mollaamin, and M. Monajjemi, Russ. Chem. Bull. **60**, 238–241 (2011). https://doi.org/10.1007/s11172-011-0039-5
61. F. Mollaamin and M. Monajjemi, J. Mol. Model. **29**, 119 (2023). https://doi.org/10.1007/s00894-023-05526-3
62. K. Bakhshi, F. Mollaamin and M. Monajjemi, J. Comput. Theor. Nanosci. **8**, 763–768 (2011). https://doi.org/10.1166/jctn.2011.1750
63. F. Mollaamin and M. Monajjemi, Int. J. Quantum Chem. **124**, e27348 (2024). https://doi.org/10.1002/qua.27348
64. L. I. Trakhtenberg, Russ. J. Phys. Chem. B **17**, 600–607 (2023). https://doi.org/10.1134/S1990793123030144
65. A. A. Shmyreva, V. E. Kirillov, E. B. Dzhangurazov, et al., Russ. J. Phys. Chem. B **17**, 764–773 (2023). https://doi.org/10.1134/S1990793123030120
66. S. N. Kozlov and B. E. Zhestkov, Russ. J. Phys. Chem. B **16**, 1030–1037 (2022). https://doi.org/10.1134/S1990793122060069
67. G. M. Khrapkovskii, I. V. Aristov, D. L. Egorov, et al., Russ. J. Phys. Chem. B **16**, 862–868 (2022). https://doi.org/10.1134/S1990793122040066
68. L. A. Wasserman, A. A. Papakhin, A. V. Krivandin, et al., Russ. J. Phys. Chem. B **16**, 141–147 (2022). https://doi.org/10.1134/S1990793122010328